PAPER

Systematic study of transport via surface and bulk states in Bi_2Te_3 topological insulator

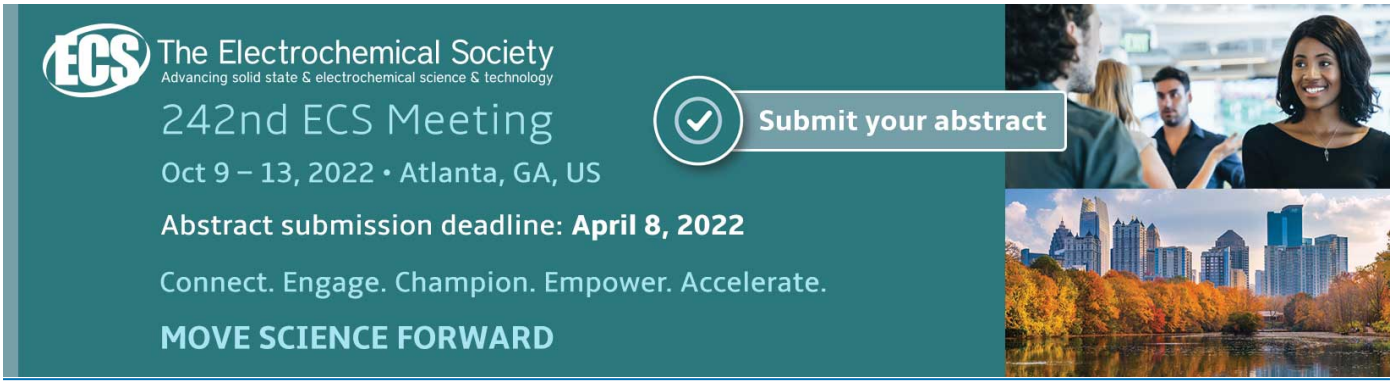

Materials Research Express

PAPER

Systematic study of transport via surface and bulk states in Bi_2Te_3 topological insulator

RECEIVED
13 April 2016

REVISED
21 June 2016

ACCEPTED FOR PUBLICATION
27 June 2016

PUBLISHED
21 July 2016

S de Castro[1], M L Peres[1], V A Chitta[2], X Gratens[2], D A W Soares[1], C I Fornari[3], P H O Rappl[3], E Abramof[3] and N F Oliveira Jr[2]

[1] Departamento de Física e Química, Universidade Federal de Itajubá, Itajubá, PB 50, MG CEP 37500-903, Brazil
[2] Instituto de Física, Universidade de São Paulo, São Paulo, PB 66318, São Paulo CEP 05315-970, Brazil
[3] Laboratório Associado de Sensores e Materiais, Instituto Nacional de Pesquisas Espaciais, São José dos Campos, PB 515, SP CEP 12201-970, Brazil

E-mail: suelenfisica@yahoo.com.br

Keywords: Bi_2Te_3, topological insulator, superconductivity, magnetoresistance

Abstract

We performed magnetoresistance measurements on Bi_2Te_3 thin film in the temperature range of $T = 1.2$–4.0 K and for magnetic fields up to 2 T. The curves exhibited anomalous behavior for temperatures below 4.0 K. Different temperature intervals revealed electrical transport through different conductive channels with clear signatures of weak antilocalization. The magnetoresistance curves were explained using the Hikami–Larkin–Nagaoka model and the 2D Dirac modified model. The comparison between the parameters obtained from the two models revealed the transport via topological surface states and bulk states. In addition, a superconductive like transition is observed for the lowest temperatures and we suggest that this effect can be originated from the misfit dislocations caused by strain, giving rise to a superconductive channel between the interface of the film and the substrate.

1. Introduction

Topological insulators (TIs) are a new class of materials that present very singular quantum–mechanical properties and have driven considerable efforts from theoreticians and experimentalists in the search of new compounds with such special properties [1–3]. The importance of TI is related to its huge potential of application in the development of spintronics and also to probe Majorana fermions in the proximity of superconductivity [3, 4].

In this search, the compound Bi_2Te_3 was identified as a three-dimensional TI, where the strong spin–orbit coupling (SOC) gives rise to insulating gapped bulk states and two-dimensional metallic surface states. The surface states present Dirac dispersions and hence the charge carriers are Dirac fermions. So far, the most reliable tool to probe the surface states through Dirac cones is performing ARPES experiments. Regarding the possible application in spintronics and other sensor devices, the detection, via transport measurements, of spin-polarized currents present in the surface states are highly desirable [5, 6].

The verification of electrical transport via topological surface states would be possible for samples with a bulk sufficiently insulating and surface carriers with high mobility. In this case, the transport would be mainly via surface states and it would be possible to verify that the carriers are Dirac fermions. However, the synthesis of such ideal sample is quite unreal due to naturally-doped bulk carriers [7]. It is important to mention that surface transport does not necessarily identify a TI and could just indicate an accumulation layer, for example, in the surface [8].

Weak localization (WL) and weak anti-localization (WAL) phenomena have been suggested as a tool to verify the existence of transport through metallic states, even when the transport occurs via bulk channels simultaneously. In non-trivial 2D system, strong SOC can produce WAL effect which causes a dip in the magnetoresistance (MR) in the region of low fields when a magnetic field is applied perpendicularly to the

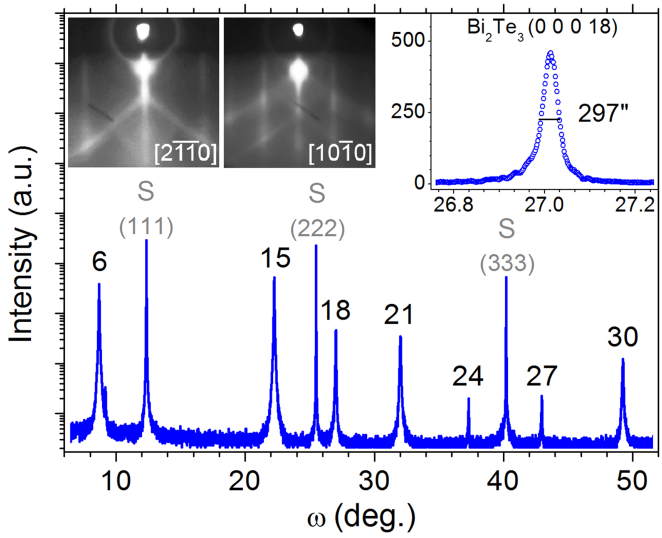

Figure 1. Wide angular $\omega/2\theta$ scan of Bi_2Te_3 epitaxial film grown on (111) BaF_2 substrate exhibiting, besides the (111), (222) and (333) BaF_2 peaks, only the (0 0 0 L) Bi_2Te_3 symmetrical diffraction peaks. On the top left inset the RHEED patterns measured along two symmetry azimuths are shown and the rocking curve measured around the $L = 18$ Bi_2Te_3 diffraction peak is exhibited on the top right inset.

sample surface [9]. In TIs, WAL effect has been widely observed and explained using the simplified Hikami–Larkin–Nagaoka (HLN) model in low field limit [3, 9–11]. A 2D modified Dirac model was recently proposed to explain the MR effect of a TI as a contribution from bulk and surface channels [12]. This model presents a description for both the surface bands and the lowest 2D bulk subbands of a TI thin film.

In this work, we report results of WAL effect observed in a 200 nm Bi_2Te_3 thin film grown on BaF_2 substrate, described in the next section. The analysis of the experimental curves was performed using both the HLN and the 2D modified Dirac models. The results of two models are very similar and show that the transport occurs via bulk and surface states. The combination of the two models revealed a powerful tool to probe the transport via surface states. In addition, a superconducting like transition is observed and we suggest that this effect can be originated from the misfit dislocations caused by strain giving rise to a superconductive channel between the interface of the film and the substrate.

2. Sample structure and experimental setup

The c-axis oriented layer of bismuth telluride (Bi_2Te_3) has been grown on a barium fluoride (BaF_2) substrate, which has the advantage of exhibiting a good match to the Bi_2Te_3 lattice constant. The lattice mismatch between the Bi_2Te_3 lattice constant and the $a_0/\sqrt{2}$ in-plane lattice constant of (111) BaF_2 substrate surface is $\Delta a/a \approx -0.05\%$ at 300 K [13, 14]. In addition, BaF_2 shows a good match of thermal expansion coefficient in relation to Bi_2Te_3. In fact, assuming a relaxed layer at room temperature, the predicted thermal strain parallel to the layer is only[4] $\varepsilon_{\parallel} = -0.026\%$ at 4.2 K [15]. In view of this, a Bi_2Te_3 film was deposited on a freshly cleaved (111) BaF_2 substrate, produced by Korth Kristalle GmbH. The growth was carried out by molecular beam epitaxy, in a Riber MBE 32P system, using a stoichiometric Bi_2Te_3 compound source. Simultaneously, an additional tellurium source was used to tune the beam flux composition and to obtain a Te-rich beam flux composition, yielding a beam flux with an overall Te/Bi_2Te_3 flux ratio equal to 2.7. As is known, a large portion of the excess Te_2 flux desorbs from the surface, and the film composition differs from the sprinkling beam flux concentration because only a small fraction of Te atoms actually incorporates in the film. Thus, the BEP (beam equivalent pressure) provided by Bi_2Te_3 source was 1.5×10^{-7} Torr and Te was 4.1×10^{-7} Torr. The substrate temperature was maintained at 280 °C and, under such conditions, either the nucleation and the growth occurs in a layer-by-layer mode. This can be evidenced at the inset panel on top left of figure 1, which exhibits the streaky patterns of reflection high-energy electron diffraction measured along two symmetry azimuths, rotated by 30° to each other. Also, no surface reconstruction of the (0 0 0 1) Bi_2Te_3 was observed and the film surface is mirror-like. As mentioned, a thin film of approximately 210 nm was deposited at a growth rate of 0.19 Å s^{-1}.

[4] The thermal strain can be calculated using $\varepsilon = \exp\int_{300\,\mathrm{K}}^{4.2\,\mathrm{K}} [\alpha_{BaF_2} - \alpha_{Bi_2Te_3}]\mathrm{d}T - 1$ and the thermal expansion coefficients (α) given in [15] for BaF_2 and in [15] for Bi_2Te_3.

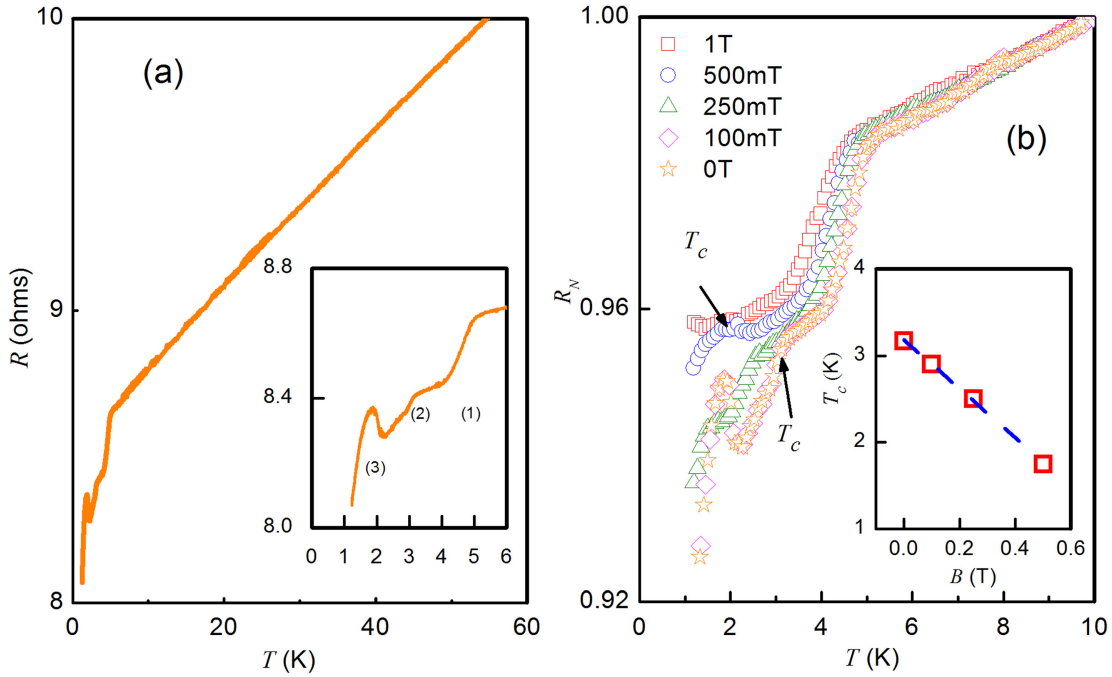

Figure 2. (a) Temperature dependence of electrical resistance of the 200 nm Bi_2Te_3 film for temperature range $T = 1.2$–60 K. Inset: three drops of resistance regions, (1), (2) and (3) at low temperatures. (b) Normalized resistance (R_N) at different applied magnetic fields. The arrows indicate the dislocation of the critical temperature T_c. Inset: critical temperature (T_c) as a function of B at which the (2) drop occurs. The values of B are higher than the values found in literature.

The structural properties of the film were investigated using a high resolution x-ray diffractometer. Figure 1 shows the diffraction curve, which presents besides the (111), (222) and (333) BaF_2 peaks only the (0 0 0 L) Bi_2Te_3 symmetrical Bragg peaks. This result indicates that the (0 0 0 L) Bi_2Te_3 hexagonal planes are parallel to the (111) substrate surface. The rocking curve measured around the (0 0 0 18) Bi_2Te_3 Bragg peak is shown on the top right inset of figure 1. The full-width at half-maximum of this curve was 297″, indicating the high structural quality of the epitaxial film.

For the electrical transport measurements, the Bi_2Te_3 sample was prepared with In contacts in Van der Pauw geometry. The measurements were performed in a 15 T He-cooled superconducting magnet, using an AC current of 1 μA at 10.7 Hz and conventional phase sensitive detection. The transport parameters were obtained using Hall technique. The carrier concentration varied from 6.7×10^{24} to 7.0×10^{24} m^{-3} for temperatures between 2.2 and 4.2 K and the carriers mobility varied from 0.85 to 0.78 $m^2\ V^{-1}\ s^{-1}$ for the same temperature range.

3. Results and discussion

The temperature dependence of the electrical resistance for the Bi_2Te_3 film was measured in the temperature range of 1.2–70 K, as presented in figure 2(a). According to this figure, the electrical resistance of the sample displays an almost linear dependence of electrical resistance with T exhibiting metallic behavior down to 5 K. This profile is expected for a degenerate semiconductor [16] and has also being observed for other TIs [17]. For temperatures below 5 K, the curve exhibits a very singular behavior where the resistance first drops slightly and then abruptly. The inset shows, in more details, three regions with different temperature dependences profiles identified as (1), (2) and (3). The last drop in region (3), in a first sight, looks like a superconductivity transition and will be discussed latter. In order to verify the possible origin of the profiles observed in the electrical resistance curve, figure 2(b) shows the temperature dependence of the normalized resistance (R_N) presented in figure 2(a) for applied magnetic fields of 1 T, 500 mT, 250 mT, 100 mT and 0 T. The drop observed in the curves in region (1) occurs for all applied magnetic fields and the slopes of the normalized resistance show weak magnetic field dependence. This behavior suggests the existence of a more conductive channel which becomes predominant, causing the drop, and has nothing to do with superconductivity effect, since the magnetic field plays no important role. In region (2), for $T \sim 3$ K, another drop occurs, but vanishes when a magnetic field is applied up to 1 T. Curiously, this effect occurs near the superconducting transition temperature of In ($T_c \approx 3$, 4 K) [18]. Similar behavior in the resistance was observed in Bi_2Te_3 samples by Hagmann *et al* [19] and Wang

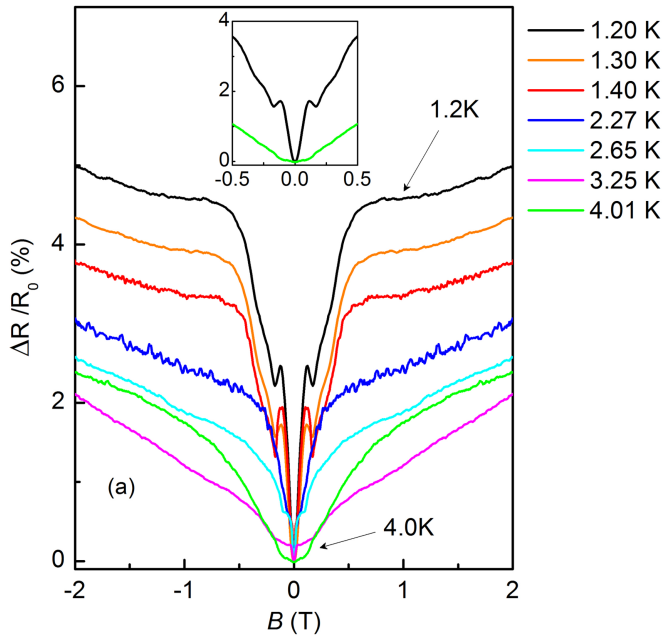

Figure 3. MR at different temperatures for magnetic fields in the range of −2 T to +2 T. The profiles of the curves in the region of low fields ($B < 1$ T) indicate the presence of SOC. Inset: MR for −500 mT to +500 mT. The profiles of the curves present huge difference, indicating a transition as the temperature diminishes form 4.0 K down to 1.2 K.

et al [20]. In both works, it was suggested that the superconductivity effect was caused the formation of a superconducting region at the In/Bi_2Te_3 interface induced by the In contacts. However, the critical magnetic field applied necessary to destroy the effect is too high as can be observed from the T_c values presented in the inset in figure 2(b). In addition, this figure shows that the critical temperature for which the drop in the electrical resistance occurs varies linearly and inversely proportional to the applied magnetic field.

In region indicated as (3), a more abruptly drop takes places and is much more similar to a superconductivity transition than the effect presented in region (2). It is well known that Bi_2Te_3 compound undergoes a superconductivity transition under hydrostatic pressure [21]. In the present case, one could expect that the thermal strain should be enough to cause the pressure and hence the superconductivity transition. However, the thermal strain is found to be weak (see the section 'sample structure and experimental setup') and cannot induce such type of transition. On the other hand, very recently, the presence of superconductivity was predicted to occur in strained Dirac materials [22] where a periodic strain could produce a flat band superconductivity regime. In our case, the interface between the substrate and the Bi_2Te_3 films could be periodically strained giving rise to a superconductivity channel responsible for the profiles observed in figure 2.

In order to observe WAL effect, we performed MR measurements in the sample. The results are presented in figure 3, with the MR curves plotted as $\Delta R/R_0 = (R(H) - R(0))/R_0$, for temperatures between 1.2 and 4.0 K and for magnetic fields in the range of −2 T to +2 T, with the magnetic field applied perpendicularly to the film surface. We have averaged over the magnetic field directions using $R_{xx} = [R(B) + R(-B)]/2$ to eliminate any Hall component. Between 0.5 and 2.0 T the MR curves exhibit similar behavior that is neither linear nor parabolic. First, for a better understanding of the profiles exhibited in this figure, we focus on the behavior of MR curves in low fields and temperatures of 2.27, 2.65 and 3.25 K, where a typical MR sharp dip is exhibited. This region corresponds to region (2) drop in resistance; inset figure 2(a). The existence of a sharp dip in MR at small fields could be associated to WAL effect attributed to the 2D Dirac surface states. The WAL effect in TIs has been described by the simplified HLN in the regions of low magnetic fields. The simplified equation can be written as [11]

$$\Delta\sigma(B) = -\frac{\alpha e^2}{\pi h}\left[\ln\left(\frac{\hbar}{4eBL_\phi^2}\right) - \psi\left(\frac{1}{2} + \frac{\hbar}{4eBL_\phi^2}\right)\right], \quad (1)$$

where e is the charge of an electron, h is the Planck's constant, L_ϕ is dephasing length, B is the magnetic field, ψ is the digamma function and α is a coefficient associated to the number of coherent channel contribution to conduction. It is known that $\alpha = -0.5$ is expected for single coherent channel or convencional 2D system with strong spin-orbit scattering. However, in our case, the simplified HLN relation cannot be the best option to fit the experimental results for two reasons: first, equation (1) is valid only in the regions of low magnetic fields and

we can observe signatures of WAL up to 0.5 T. Second, in the region of low magnetic fields, the effect seems to be a mixture of WAL and some other anomalous effect, as observed in figure 2. Hence, we used to describe the data the original HLN equation [23, 24]

$$\Delta\sigma(B) = \sum_{i=0,1} -\frac{\alpha_i e^2}{\pi h}\left[2\eta\left(\frac{\hbar}{4eL_e^2 B}\right) - 2\eta\left(\frac{B^z_{soi} + 2B^x_{soi} + B_{\phi i}}{B}\right) + \eta\left(\frac{B_{\phi i}}{B}\right) - \eta\left(\frac{4B^x_{soi} + B_{\phi i}}{B}\right)\right] \quad (2)$$

where $\eta(x)$ is defined as $\eta(x) = \left[\psi\left(x + \frac{1}{2}\right) - \ln(x)\right]$ and is L_e is the electron mean free path. The free parameters are the dephasing field ($B_{\phi i}$) and spin orbit fields in x (B^x_{soi}) and z (B^z_{soi}) directions. In this case, the x direction is in the plane and z direction is normal of the surface. Equation (2) can be rearranged to take in account the sum of WAL and WL effects separately, where α_i is positive for WL ($i = 0$) and negative for WAL ($i = 1$). The sum the both effects was already used to analyze MR curves observed in SnTe films [25]. In addition, we considered $B_{\phi 0} = B_{\phi 1}$ since there is no reason to believe that the dephasing mechanism would be different in two metallic channels.

The best fitting of magnetoconductance by HLN model (dash lines) performed at 2.27 K , 2.65 K and 3.25 K temperatures are presented in figures 4(a)–(c), respectively, where the experimental points are represented by open symbols. The fitting parameters are shown in table 1. For the fitting, we wrote the magnetoconductivity as $(\sigma - \sigma_0)/\sigma_0$, where $\sigma = 1/\rho$ and $\sigma_0 = 1/\rho_0$. We have obtained $\alpha_0 \sim 0.52$ and $\alpha_1 \sim -0.55$. These values indicated the presence of two channels contributions to the transport. Other combinations of α parameter lead to very unrealistic values of spin–orbit fields and less reliable fittings. The values of α are in accordance to recent experiments where α values obtained from equation (1) cover a range between -0.39 and -0.54 at 2 K [21, 26, 27].

The lengths associated with dephasing and spin–orbit fields were derived from the fitting parameters, presented in table 1, according to the relation $B_n = \hbar/4eL_n^2$, where $n = \phi$, so^x, so^z and are presented in table 2. $L_e \approx 25$ nm was calculated from the transport measurements presented in section 2. The $L_{\phi 0}$, $L_{\phi 1}$, L^x_{so0}, L^x_{so1} and L^z_{so0} values are nearly constant in the temperature range studied. At 2.27 K (3.25 K) we obtained $L_{\phi 0} = L_{\phi 1} = L_\phi = 582$ nm (547 nm) which is comparable to $L_\phi = 331$ nm, estimated from simplified HLN model to Bi_2Te_3 films [27]. Furthermore, the condition $L_\phi \gg L_e$, referring to diffusive regime, where WAL or WL effects are observed, is satisfied. On the other hand, according to table 2, $L^x_{so0} \sim L^x_{so1}$, indicating that SO coupling has the same intensity in the two channels. In addition, from table 2, we observe that $L^z_{soi} > L^x_{soi}$, indicating that the SO coupling is more effective in x direction. The values of L^z_{so1} are the order of magnitude of the sample thickness, indicating 2D behavior.

The analysis performed using HLN model provides a good comprehension of the SOC effect and suggests that the profiles observed in the MR curves in the low field region could be originated from two channels contribution. It is worth to compare the results presented so far with the analysis performed using a model that distinguishes between surface and bulk channels transport. This can be done making use of the 2D modified Dirac model [12]

$$\Delta\sigma(B) = \sum_{i=0,1} \frac{f_i \alpha_i e^2}{\pi h}\left[\psi\left(\frac{L_B^2}{L_{\phi i}^2} + \frac{1}{2}\right) - \ln\frac{L_B^2}{L_{\phi i}^2}\right]. \quad (3)$$

Equation (3) provides a unified description for 2D bulk subbands due to the quantum confinement and the surface bands of a 3D TI. In this equation L_B is the magnetic length, f_i is a multiplicative constant, introduced to account for possible multichannel conduction and $1/L_{\phi i}^2 = 1/L_\phi^2 + 1/L_i^2$.

Figures 4(a)–(c) show the fitting obtained by equation (3) (solid lines). $\alpha_{0,1}$, L_ϕ and $L_{\phi 0,1}$ are in table 3 and they were derived from the fitting parameter, cos Θ_i, that control the crossover from WL to WAL. In fact, using this model and considering two conduction channels, only two fitting parameters are necessary: cos θ_0, for bulk channels, and cos θ_1, for surface channels (see [12] for more details).

Our experimental values of $|\alpha|$ changed from $\approx$0.29 to $\approx$0.49 as T is increased from 2.27 to 3.25 K. This considerable change in α parameter, in such a short temperature interval, seems to be unnatural. However, the anomalous drops observed in figure 2, in region (2), occur in this same temperature range. This is also a good indication of conduction through more than one channel. In addition, according to Lu *et al* [12] the value of $\alpha = -0.5$ does not always mean that there is only one surface channel, instead, it could also indicate a collective result of multiple surface and bulk channels. For the fittings presented in figure 4, using the 2D Dirac model, we

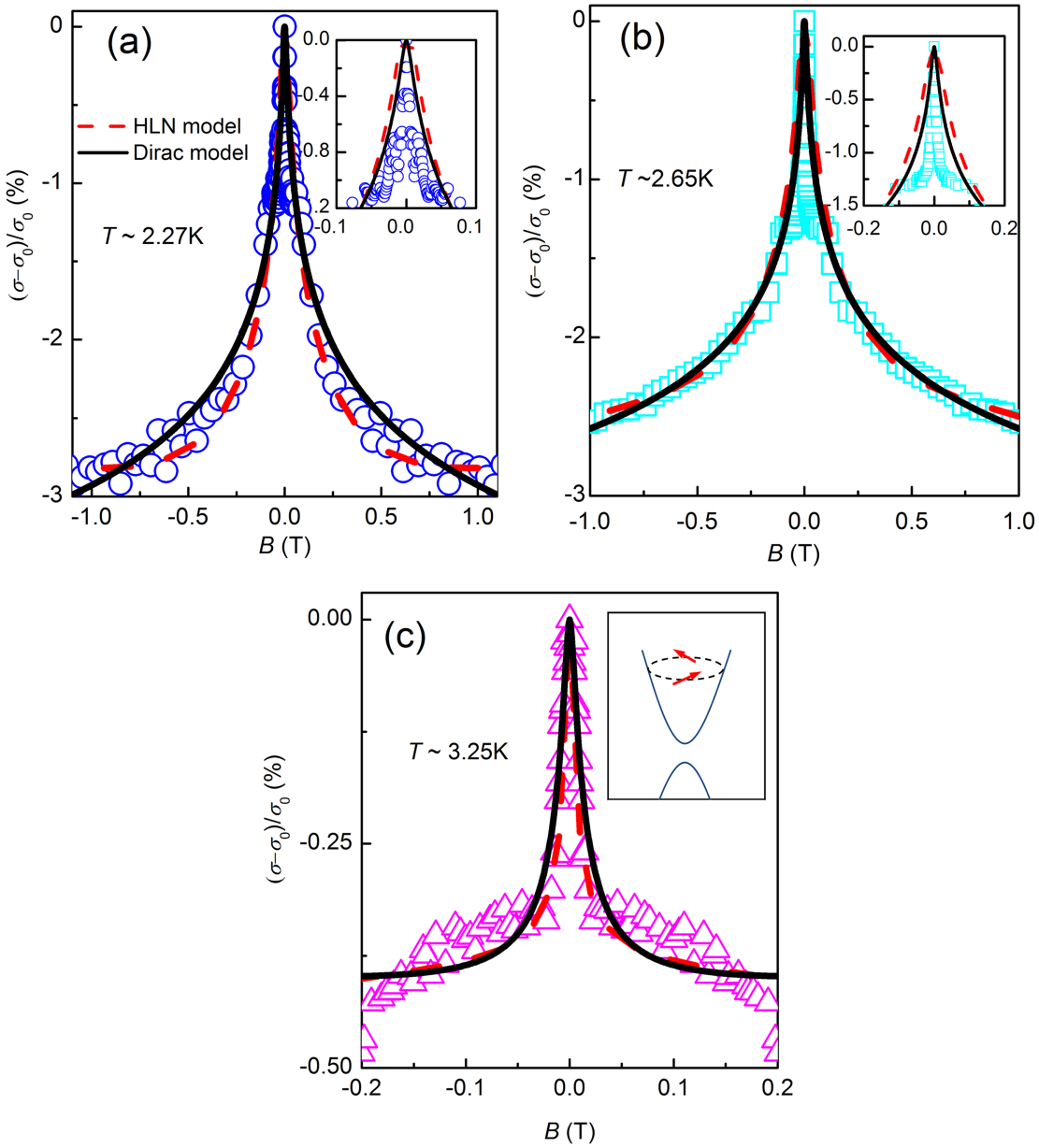

Figure 4. HLN (dash line) and 2D modified Dirac model (solid line) fits of magnetoconductance at (a) 2.27 K , (b) 2.65 K and (c) 3.25 K. The experimental points are represented by open symbols. The insets in figures (a) and (b) are the zoom views at low fields, where the models cannot be applied, and the inset in figure (c) is the schematic view of the partial polarization of the spins in the conduction band.

Table 1. Fitting parameters obtaining from HLN model, with constant α_i, dephasing field B_ϕ and spin-orbit field B_{soi} in x and z directions ($i = 0$ or 1 for WL or WAL, respectively).

T(K)	α_0	α_1	B_ϕ (mT)	B^x_{so0} (T)	B^x_{so1} (T)	B^z_{so0} (T)	B^z_{so1} (T)
2.27	0.52	−0.55	0.97	0.75	0.89	0.09	0.01
2.65	0.52	−0.55	0.97	0.55	0.80	0.09	0.01
3.25	0.52	−0.55	1.1	0.89	0.38	0.09	0.09

used $f_0 = f_1 = 1$, which means that considering only one surface channel and one bulk channel was enough to perform the fittings. This is coherent with the analysis performed using the HLN model.

The fittings obtained using HLN and 2D modified Dirac model presented coherent parameters that are consistent to the data found in literature. The Dirac model is more accurate, since it takes into account the surface states while HLN makes no distinction about the origin of WAL effect. In addition, it is possible to verify

Table 2. The dephasing length ($L_{\phi i}$), spin–orbit coupling length (L^x_{soi}, L^z_{soi} in x and z directions) calculated from fitting parameters from HLN model ($i = 0$ or 1 for WL or WAL, respectively).

T(K)	$L_{\phi 0}$ (nm)	$L_{\phi 1}$ (nm)	L^x_{so0} (nm)	L^x_{so1} (nm)	L^z_{so0} (nm)	L^z_{so1} (nm)
2.27	582	582	20.9	19.2	60.5	181
2.65	582	582	24.5	20.3	60.5	181
3.25	547	547	19.2	21.5	60.5	60.5

Table 3. Coefficient (α), $1/L^2_{\phi i} = 1/L^2_{\phi} + 1/L^2_i$ length, fitting parameters cos Θ from the 2D modified Dirac model, and multiplicative constant f.

T(K)	α_0	α_1	L_{ϕ} (nm)	$L_{\phi 0}$ (nm)	$L_{\phi 1}$ (nm)	cos Θ_0	cos Θ_1	$f_{0,1}$
2.27	0.29	0.31	250	216	222	0.34	0.29	1
2.65	0.30	0.31	250	217	223	0.35	0.30	1
3.25	0.49	0.49	250	245	249	0.80	0.053	1

the spin polarization deriving the relation cos $\Theta_i(\varepsilon_F - Dk_F^2)$ (see [12]), where ε_F the Fermi energy, k_F is the Fermi wave vector and D is a theoretical parameter in the model. We found that cos $\Theta_i(\varepsilon_F - Dk_F^2) < 0$ ($\sim -10^{-3}$ eV) for all the temperatures analyzed. This result indicates that the carriers spins are only partially polarized in the conduction band, as presented schematically in the inset of figure 4(c). Actually, this behavior is expected since scattering originated from the bulk states leads to the reduction of spin polarization of the surface states [28]. Hence, even if there is transport via surface states, the spin polarization is affected due to the interaction with states from the bulk. This could be an important issue for the development of spintronic devices based on this material and should be taken into account for future applications.

For magnetic fields below 100 mT, an additional effect is clearly present (see inset in figures 4(a) and (b)). This region seems to be in a transition region between the metallic and a superconductivity phase and the models used here are not suitable for an analysis in this region. Also, the models where able to fit only a small range in magnetic field for $T \sim 3.25$ (figure 4(c)). This can be associated to the transition region (identified as region (2) earlier) where the models also cannot take into account all the specific features present in the system.

In fact, for the temperatures 1.2 , 1.3 and 1.4 K it is not possible to fit the magnetoconductance curves with the models in any range of magnetic fields. These temperatures are in region (3), as indicated in figure 2(a), where the superconductive like phase is present.

In conclusion, we presented magnetotransport measurements performed on a 200 nm Bi_2Te_3 film. The experimental curves showed anomalous behavior for temperatures below 4 K. The drops in the resistance versus temperature curve, for temperatures higher than 2.0 K, indicated the presence transport in more than one metallic channel. The detailed analysis performed using the HLN and 2D Dirac models indicated that transport occurs via surface and bulk states. The analysis performed making use of the two models represents a more reliable procedure in order to identify the transport via surface states. For the lowest temperatures measured, a superconductivity phase like appears and does not permit a further analysis using the theoretical models. We suggest that superconductivity effect is originated from the strain between the interface on the film and the substrate according the recent theoretical predictions. These results shed some light about the electrical transport via surface and bulk states in Bi_2Te_3 TI.

The authors would like to thank CAPES, FAPEMIG (APQ-00623-14) and FAPESP (2007/50968-0) for financial support.

References

[1] Yan C *et al* 2014 *Phys. Rev. Lett.* **112** 186801
[2] Safaei S, Kacman P and Buczko R 2013 *Phys. Rev.* B **88** 045305
[3] Veldhorst M, Snelder M, Hoek M., Molenaar C G, Leusink D P, Golubov A A, Hilgenkamp H and Brinkman A 2013 *Phys. Status Solidi RRL* **7** 26
[4] Ando Y 2013 *J. Phys. Soc. Japan* **82** 102001
[5] Hasan M Z and Kane C L 2010 *Rev. Mod. Phys.* **82** 3045
[6] Barua S, Rajeev K P and Gupta A K 2015 *J. Phys.: Condens. Matter* **27** 015601
[7] Dziawa P *et al* 2012 *Nat. Mater.* **11** 1023
[8] von Klitzing K and Landwehr G 1971 *Solid State Commun.* **9** 2201
[9] Taskin A A, Sasaki S, Segawa K and Ando Y 2012 *Phys. Rev. Lett.* **109** 066803
[10] Wang J, DaSilva A M, Chang C Z, He K, Jain J K, Samarth N, Ma X C, Xue Q K and Chan M H W 2011 *Phys. Rev.* B **83** 245438
[11] Roy A, Guchhait S, Sonde S, Dey R, Pramanik T, Rai A, Movva H C P, Colombo L and Banerjee S K 2013 *Appl. Phys. Lett.* **102** 163118
[12] Lu H Z and Shen S Q 2011 *Phys. Rev.* B **84** 125138

[13] Hellwege K H 1973 *Landolt-Börnstein, Numerical Data and Functional Relationships in Science and Technology* (*New Series* group lll) (Berlin: Springer) vols 1–9
[14] Nakajima S 1963 *J. Phys. Chem. Sol.* **24** 479
[15] White G K 1980 *J. Phys. C: Solid State Phys.* **13** 4905
Barnes J O, Rayne J A and URE R W Jr 1974 *Phys. Lett.* **46A** 317
[16] Liu M *et al* 2011 *Phys. Rev.* B **83** 165440
[17] Balakrishnan G, Bawden L, Cavendish S and Lees M R 2013 *Phys. Rev.* B **87** 140507
[18] Eisenstein J 1954 *Rev. Mod. Phys.* **26** 277
[19] Hagmann J A, Liu X, Dobrowolska M and Furdyna J K 2013 *J. Appl. Phys.* **113** 17C724
[20] Wang Z, Ye T and Mani R G 2015 *Appl. Phys. Lett.* **107** 172103
[21] Manjón F J *et al* 2013 *Phys. Status Solidi* b **250** 669
[22] Kauppila V J, Aikebaier F and Heikki T T 2016 *Phys. Rev.* B **93** 214505
[23] Hikami S, Larkin A I and Nagaoka Y 1980 *Prog. Theor. Phys.* **63** 707
[24] Zhang S X, McDonald R D, Shekhter A, Bi Z X, Li Y, Jia Q X and Picraux S T 2012 *Appl. Phys. Lett.* **101** 202403
[25] Akiyama R, Fujisawa K, Sakurai R and Kuroda S 2014 *J. Phys.: Conf. Ser.* **568** 052001
[26] Chiu S P and Lin J J 2013 *Phys. Rev.* B **87** 035122
[27] He H T, Wang G, Zhang T, Sou I K, Wong G K L, Wang J N, Lu H Z, Shen S Q and Zhang F C 2011 *Phys. Rev. Lett.* **106** 166805
[28] Neupane M *et al* 2013 *Nat. Commun.* **5** 3841